CONDENSED MATTER PHYSICS

Strain and vector magnetic field tuning of the anomalous phase in $Sr_3Ru_2O_7$

Daniel O. Brodsky,[1,2] Mark E. Barber,[1,2] Jan A. N. Bruin,[2,3] Rodolfo A. Borzi,[4] Santiago A. Grigera,[2,4] Robin S. Perry,[5] Andrew P. Mackenzie,[1,2]* Clifford W. Hicks[1]*

A major area of interest in condensed matter physics is the way electrons in correlated electron materials can self-organize into ordered states, and a particularly intriguing possibility is that they spontaneously choose a preferred direction of conduction. The correlated electron metal $Sr_3Ru_2O_7$ has an anomalous phase at low temperatures that features strong susceptibility toward anisotropic transport. This susceptibility has been thought to indicate a spontaneous anisotropy, that is, electronic order that spontaneously breaks the point-group symmetry of the lattice, allowing weak external stimuli to select the orientation of the anisotropy. We investigate further by studying the response of $Sr_3Ru_2O_7$ in the region of phase formation to two fields that lift the native tetragonal symmetry of the lattice: in-plane magnetic field and orthorhombic lattice distortion through uniaxial pressure. The response to uniaxial pressure is surprisingly strong: Compressing the lattice by ~0.1% induces an approximately 100% transport anisotropy. However, neither the in-plane field nor the pressure phase diagrams are qualitatively consistent with spontaneous symmetry reduction. Instead, both are consistent with a multicomponent order parameter that is likely to preserve the point-group symmetry of the lattice, but is highly susceptible to perturbation.

INTRODUCTION

In "correlated electron" metals, the interactions between conduction electrons are strong and, at low temperatures, can drive spontaneous self-organization into ordered states, such as superconductivity and various types of magnetic order. This is analogous to the self-organization of atoms into crystals when a liquid solidifies, but arguably with a wider range of possibilities due to the enhanced role of the effects of quantum mechanics. One particularly intriguing possibility is that, solely through the effects of electron-electron interactions, a preferred direction of conduction is established. This occurs when electronic order with twofold rotation symmetry (C_2 symmetry) is established on an otherwise fourfold rotationally symmetric (C_4 symmetry) lattice, as is suspected or demonstrated to occur in cuprate (*1*, *2*) and iron-based superconductors (*3*, *4*), a nematic quantum Hall state in GaAs two-dimensional (2D) electron gases (*5*, *6*), the hidden order phase of URu_2Si_2 (*7*), and the superconductivity of $Cu_xBi_2Se_3$ (*8*). It has been suspected for a well-known electronic phase in $Sr_3Ru_2O_7$ (*9*–*11*).

Apart from cataloging possible types of order, it is also of broad interest to understand the general conditions under which electronic order can occur. In metals such as copper, the interaction energy is low compared with the zero-point kinetic energy of the charge carriers, and no ordered state is observed down to the lowest temperatures measured so far. In many cuprates, interactions are very strong, and the resulting ordered phases condense at relatively high temperatures and are robust against perturbation. This robustness is useful for applications but a hindrance for understanding: External stimuli, such as laboratory-accessible magnetic fields and pressures, do not have much effect. $Sr_3Ru_2O_7$ lies between these extremes. Electronic correlations are strong, as evidenced by a large mass renormalization and Wilson ratio (*12*, *13*), inelastic neutron scattering data (*14*), and the induction of localized spin density wave order by certain impurities (*15*, *16*). However, the electronic order that results is fragile. It does not appear at ambient pressure and magnetic field but instead only in a narrow window of applied fields near 8 T (*10*).

Electrical conduction in $Sr_3Ru_2O_7$ takes place mainly in Ru–O bilayers. Interlayer coupling leads to substantial bilayer splitting of parts of the electronic structure, but the bilayers are weakly coupled, and the Fermi surfaces are quasi-2D (*12*, *17*). When magnetic field is applied along the *c* axis (perpendicular to the Ru–O bilayers), a metamagnetic transition (a field-induced jump in the magnetization) occurs at around 8 T. In moderately clean samples, with residual resistivity ~1 microhm·cm and above, it is a single transition. Metamagnetic transitions are first-order; however, the critical end point of this transition is located at ~0 K (*18*), making it a quantum critical end point. In samples with residual resistivity below 1 microhm·cm, the metamagnetic transition splits into two first-order transitions, at ≈7.9 and ≈8.1 T, and an ordered phase, marked by enhanced resistivity, occurs in their vicinity and below 1.1 K (*9*, *10*). In other words, soft modes associated with the quantum critical end point appear to nudge the system into an ordered state, and the precise connection between the quantum criticality and condensation of order has been the subject of considerable study (*19*–*23*). This ordered state can be strongly modified by laboratory-accessible magnetic fields and modest uniaxial pressures, as shown here. This perturbability and the extremely low disorder (micrometer-scale mean free paths are achievable) make $Sr_3Ru_2O_7$ an ideal system for study.

Two key observations suggest that the ordered phase spontaneously breaks the tetragonal symmetry of the lattice. One is that the resistivity enhancement in the phase is around 100% in the absence of in-plane magnetic fields. This is a strikingly large value and suggests an additional elastic scattering channel, which could be walls between domains of different orientations of the order (*10*, *24*). The other observation is that, within the phase, a modest in-plane magnetic field, applied along a ⟨100⟩ lattice direction, induces strong resistive anisotropy between the (100) and (010) directions (that is, the *x* and *y* directions), suggesting reorientation of either the order itself or the domain walls (*9*, *11*). (We

[1]Max Planck Institute for Chemical Physics of Solids, Nöthnitzer Straße 40, 01187 Dresden, Germany. [2]Scottish Universities Physics Alliance, School of Physics and Astronomy, North Haugh, University of St Andrews, St Andrews KY16 9SS, U.K. [3]Max Planck Institute for Solid State Physics, Heisenbergstraße 1, 70569 Stuttgart, Germany. [4]Instituto de Física de Líquidos y Sistemas Biológicos, Universidad Nacional de La Plata–Consejo Nacional de Investigaciones Científicas y Técnicas, 1900 La Plata, Argentina. [5]London Centre for Nanotechnology, University College London, Gower Street, London WC1E 6BT, U.K.
*Corresponding author. Email: mackenzie@cpfs.mpg.de (A.P.M.); hicks@cpfs.mpg.de (C.W.H.)

work throughout this paper with tetragonal notation for $Sr_3Ru_2O_7$, where the ⟨100⟩ directions are the Ru–O–Ru bond directions. In reality, $Sr_3Ru_2O_7$ has a slight orthorhombicity, with ⟨110⟩ principal axes (*25*–*27*). However, electrical transport in zero field has been found to be isotropic to high precision (*28*); thus, for simplicity, we refer to $Sr_3Ru_2O_7$ as tetragonal.) Motivated by these observations, the phase has been considered a candidate for nematic order (that is, the point-group symmetry of the lattice is lifted but translation symmetry is preserved), and several models for nematic Fermi surface distortions in $Sr_3Ru_2O_7$ have been proposed (*29*–*33*).

A recent landmark neutron scattering study reported the discovery of spin density wave order within the phase: There are scattering peaks at $(\pm q, 0, 0)$ and $(0, \pm q, 0)$, with q incommensurate and taking on slightly different values above and below the second metamagnetic transition (at 8.1 T) (*34*). The observed phase boundaries are in agreement with those seen in transport and thermodynamic studies (*10*). Most of the models for nematicity in $Sr_3Ru_2O_7$ are based on $q = 0$ interorbital and intraorbital interactions, and although it remains possible that these interactions play an important role in phase formation, the neutron data establish that $q \neq 0$ interactions are also present.

A clear understanding of the possible electronically induced C_4 to C_2 symmetry reduction is of broad importance because of the growing range of materials (some of which are listed above) where it is likely to occur. An essential question is to distinguish between a large but finite susceptibility toward C_2 symmetry (meaning that small but nonvanishing symmetry-breaking fields induce strong anisotropy), which in principle is possible with a C_4-symmetric ground state, and truly spontaneous C_2 symmetry. This can be technically difficult: It is clear from existing knowledge of $Sr_3Ru_2O_7$ that if the anomalous phase region is spontaneously C_2-symmetric, then it must generally contain domains of both possible orientations (*9*), and a noninfinitesimal applied field might be required to fully orient all the domains. However, it is important to precisely probe this question, both for general understanding and to constrain microscopic theories for $Sr_3Ru_2O_7$. The neutron study does not address this question because the scattering peaks could arise from either separate domains of (100)- and (010)-oriented spin density waves, or their microscopic coexistence. Thermodynamic measurements do not offer a definitive resolution either: Although the transition into the phase as the temperature is reduced is well established to be second-order (*10*, *35*, *36*), indicating a broken symmetry, it could be the translation symmetry breaking, as indicated by the neutron data, and not necessarily C_4 to C_2 symmetry.

Here, we investigate using two complementary probes that lift the native tetragonal symmetry of the lattice. First, we apply both compressive and tensile in-plane uniaxial pressure to induce orthorhombic lattice distortion. We find that small lattice distortions can markedly enhance the phase. Second, for a gentler and more precise perturbation, we use a vector magnet to study the response to modest, precisely controllable in-plane fields, paying particular attention to the investigation of field training and hysteretic effects. The results place strong constraints on the energetics of possible domain formation, and yield phase diagrams pointing to a multicomponent order parameter that might not break the C_4 point-group symmetry of the lattice.

RESULTS

Uniaxial pressure

Previous research has shown that hydrostatic pressure increases the metamagnetic transition fields of $Sr_3Ru_2O_7$ (*37*, *38*), whereas uniaxial pressure along the c axis reduces the transition fields and eventually induces ferromagnetism (*39*). In-plane uniaxial pressure experiments have not been reported, although a theoretical study found that nematic transitions may show first-order Griffiths wings in the presence of applied anisotropy (*40*).

We used a piezoelectric-based apparatus that can both compress and tension test samples (*41*). Samples were prepared as beams and secured with epoxy across a gap of width ~1 mm. Piezoelectric actuators strained the sample by minutely varying the width of this gap. An image and a schematic of a mounted sample are shown in Fig. 1. High strain homogeneity is important to keep transitions reasonably narrow as strain is applied; thus, samples were prepared with high length-to-width and length-to-thickness aspect ratios to reduce end effects. In addition, the bonding to the sample ends was (approximately) symmetric between the upper and lower surfaces; asymmetry could cause the sample to bend as pressure is applied, imposing a strain gradient across the sample thickness (*41*).

Because the center of the sample is free, the transverse strains are set by the Poisson's ratios of $Sr_3Ru_2O_7$. Compression along **a**, for example, induces expansion along **b**; thus, the applied strain induces strong orthorhombic distortion. Both the neutron scattering peaks and transport data indicate ⟨100⟩ (that is, Ru–O–Ru bond directions) principal axes for the strong C_2 susceptibility of the phase: Within the phase, an in-plane field along (100) induces strong resistive anisotropy between the (100) and (010) directions, whereas a (110) field induces very little (110)/(1$\bar{1}$0) anisotropy. Therefore, samples were cut (and the pressure was applied) along ⟨100⟩ directions. Three samples were strained and yielded consistent results. They were cut from the same crystal because our aim was to test our results against variability of the mounting conditions, rather than crystal-to-crystal variability. The parent crystal has previously been thoroughly characterized with transport, magnetization, and de Haas–van Alphen experiments (*42*).

Six electrical contacts were made to each sample, as illustrated in Fig. 1A. Longitudinal resistivity ρ_{aa} was measured by running current through contacts 1 and 2 and measuring voltage between contacts 5 and 6 or between contacts 3 and 4. The zero-field residual resistivity of the samples was found to be ≈0.5 microhm·cm. A qualitative measure of the transverse resistivity, ρ_{bb}, was obtained for two samples by

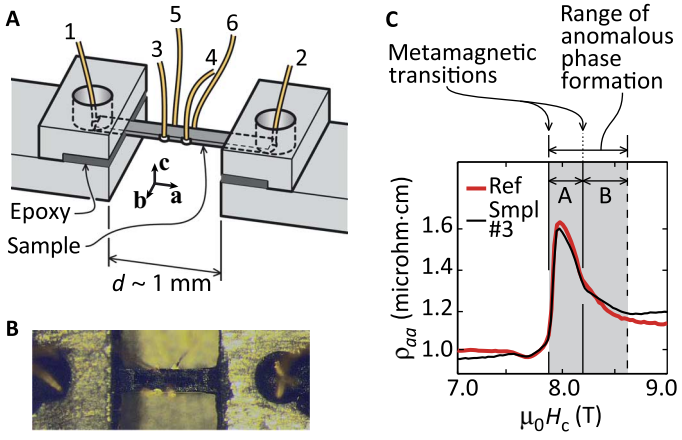

Fig. 1. Sample setup for strain tuning. (**A** and **B**) Schematic illustration and image of a mounted sample. Strain was applied by minutely varying the gap width d. (**C**) ρ_{aa} against H_c, where **H** = (0, 0, H_c), of a zero-strain reference sample, and strained sample (Smpl) #3 mounted in the strain apparatus and tuned to near-zero strain. $T \approx 300$ mK.

passing current through contacts 3 and 5 and measuring voltage between contacts 4 and 6. It is only qualitative because (i) the current flow is not homogeneous, so the measured voltage has some dependence on ρ_{aa}, and (ii) uncertainty in the true contact geometry prevented accurate calculations to extract ρ_{bb}. In addition, on one sample, a strong field-dependent but strain-independent background appeared in the transverse response, which was later found to originate in vibration of the transverse leads.

Figure 1C shows ρ_{aa} against the *c*-axis field for a zero-strain reference sample, cut from the same original crystal as the strained samples and mounted on flexible wires to avoid thermal stresses. ρ_{aa} of a strained sample is also shown, with the strain adjusted to match the reference as closely as possible. Phase formation occurs between 7.9 and ≈8.6 T. The lower boundary coincides with the first metamagnetic transition. There is a clear resistive anomaly associated with the second metamagnetic transition at ≈8.1 T, which separates regions of the phase denoted A and B. The existence of the B region is indicated by transport, thermal expansion, and neutron scattering measurements (*28*, *34*, *36*); however, the thermodynamic signatures of phase formation are much weaker than those of the A region (*43*).

Figure 2A shows ρ_{aa} of a strained sample at $T \approx 300$ mK at a series of applied longitudinal strains ε_{aa}. The origin of the strain scale is determined through comparison with the reference, to within an estimated error of ±0.01% strain. (See Materials and Methods for further discussion of error in the strain.) ε_{aa} was incremented at 7 T, outside the field range for phase formation. This is important because if there is spontaneous symmetry breaking, then varying ε_{aa} while within the phase could induce metastable domain configurations. The data show that, under compression, ρ_{aa} increases strongly and that the field range of ρ_{aa} enhancement expands. Under 0.2% compression, phase formation, as identified by enhanced ρ_{aa}, extends from 7.7 to 9.3 T. On the other hand, a tension of only 0.05% eliminates the phase-induced enhancement of ρ_{aa}.

The transverse response (after background subtraction) is shown in Fig. 2B. It increases strongly when the sample is tensioned, which indicates strongly increased ρ_{bb}: Although the transverse response is also affected by ρ_{aa}, ρ_{aa} is suppressed to a nearly constant base value under strong tension, and so cannot account for this response. In summary, compression along **a** increases ρ_{aa}, and tension along **a** increases ρ_{bb}.

Contour plots of the longitudinal and transverse responses are shown in Fig. 3 (A and B, respectively); contour plots for another strained sample are shown in the Supplementary Materials. The longitudinal and transverse responses approximately mirror each other, and for each, there is a region of strongly enhanced response that indicates phase formation. Taking a fixed contour level as an approximate criterion for the boundaries of these regions yields the phase diagram shown in Fig. 3C. A notable feature of Fig. 3C is the existence of a region of overlap, with a maximum width of ≈0.08% strain. This overlap suggests that the order has two components that can be simultaneously nonzero, which is evidence for a multicomponent order parameter. This is covered more thoroughly in Discussion.

We conclude our presentation of strain-tuning data by showing the effect of strain over a wider field range in Fig. 4A. Outside the phase formation region, the strain response is nearly linear over the applied strain range; thus, the normalized linear elastoresistance, $(1/R)dR/d\varepsilon_{aa}$, determined at $\varepsilon_{aa} = 0$, is plotted in the figure. The change in sample dimensions yields a geometric contribution to the elastoresistance even when the resistivity does not change. For isotropic materials with Poisson's ratio ν, this geometric contribution is 1 + 2ν, typically ~2,

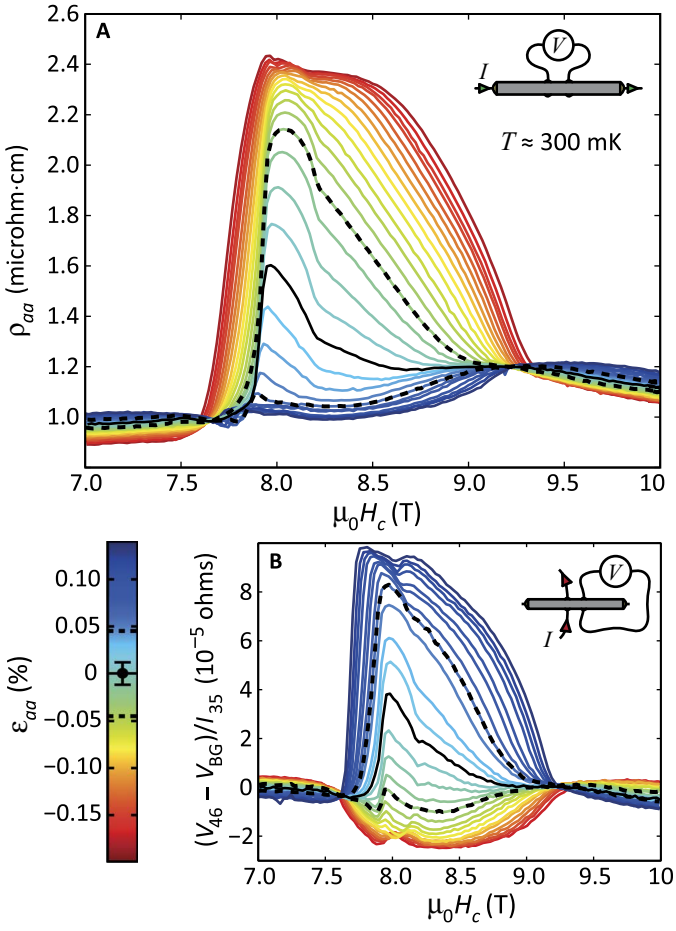

Fig. 2. Strain-tuning results. (**A**) Longitudinal resistivity ρ_{aa} against the *c*-axis field for sample #3, at a series of applied strains ε_{aa}. **H** = (0, 0, H_c), $T \approx 300$ mK. The measurement configuration is shown on the top right. (**B**) Transverse response for the same sample. V_{46} is the voltage between contacts 4 and 6; V_{BG} is the background, which is determined by fits to V_{46} outside the region of phase formation; and I_{35} is the current between contacts 3 and 5. (Contact numbering is shown in Fig. 1A.)

and for ordinary metals it is typically the dominant contribution (*44*). The elastoresistance can be higher in narrow-band metals (where the overlap between orbitals on adjacent sites is weak, and can be highly perturbable), and in materials with strong electronic correlations (*4*). $Sr_3Ru_2O_7$ is known to be both narrow-band and strongly correlated, which is consistent with the observation of $(1/R)dR/d\varepsilon_{aa} \sim 20$ far from the phase: a much smaller elastoresistance than within the phase, but still large. Note that the elastoresistance is nearly zero at 7.6 and 9.2 T, a feature that appears as crossing points in Fig. 2A. The data in Fig. 4B show that, at these fields, ρ_{aa} is nearly strain-independent for $|\varepsilon_{aa}|$ up to ~0.1%. This appears to reflect a balance between the positive elastoresistance outside the phase and the strongly negative elastoresistance within, and it will be interesting to more carefully examine these points in the future.

Vector field

Another way to lift C_4 symmetry is with a vector magnetic field, **H** = (H_a, H_b, H_c). Recently published vector field results showed that the high susceptibility to in-plane fields of the A phase is shared by the B phase (*28*). The vector magnet used in both that study and in the present work can apply H_c to 8.5 T, simultaneously with $\sqrt{(H_a^2 + H_b^2)}$ up to

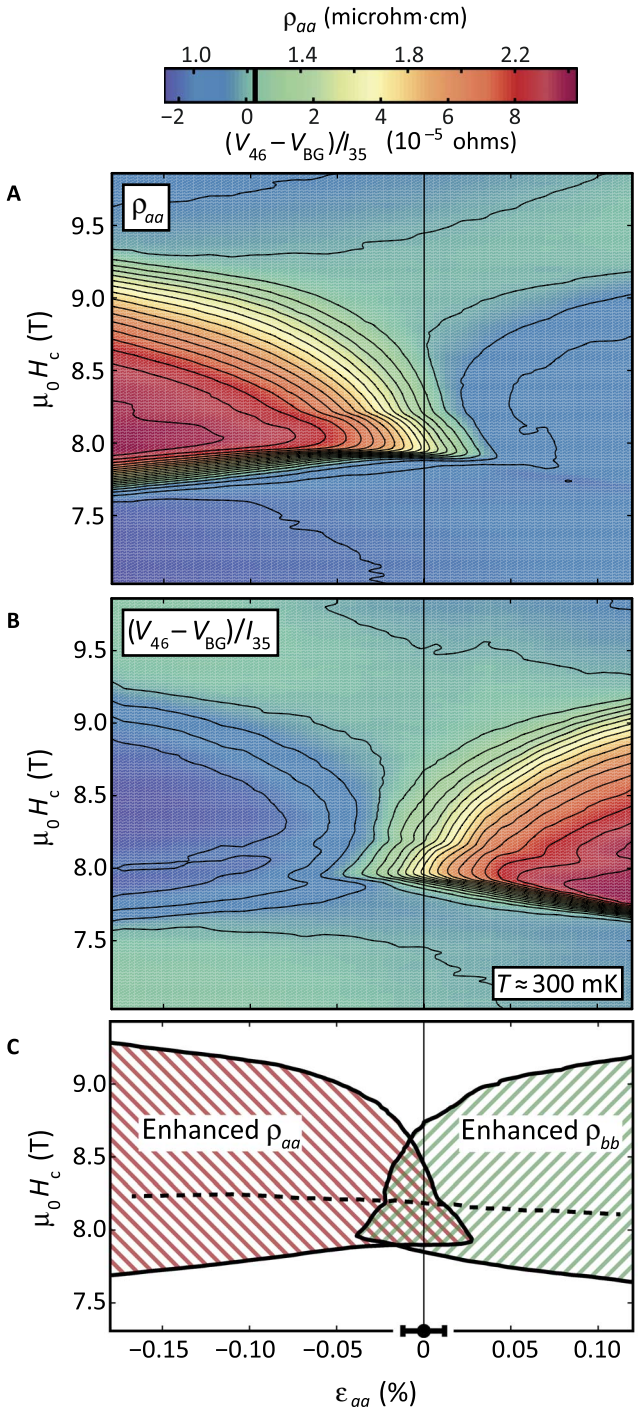

Fig. 3. Strain-tuning contour plots. (**A** and **B**) Contour plots of the longitudinal and transverse response, respectively, of sample #3 as a function of *c*-axis magnetic field and sample strain. **H** = (0, 0, H_c), $T \approx 300$ mK. (**C**) Outlines of the regions of enhanced ρ_{aa} and ρ_{bb}. For convenience, these outlines are taken as the contour level indicated by the heavy black line in the scale bar. The dashed line is the cusp in the resistance versus field curves, which at zero strain is associated with the second metamagnetic transition. The error bar on the *x* axis indicates the error in our determination of zero strain. Although this phase diagram indicates a small asymmetry about zero strain that suggests spontaneous C_4 symmetry breaking, it should be treated with care. Within error, the measurement is consistent with C_4 symmetry being respected at zero strain, and previous measurements on entirely strain-free samples have shown C_4-symmetric transport in the absence of in-plane magnetic fields (*11*, *28*).

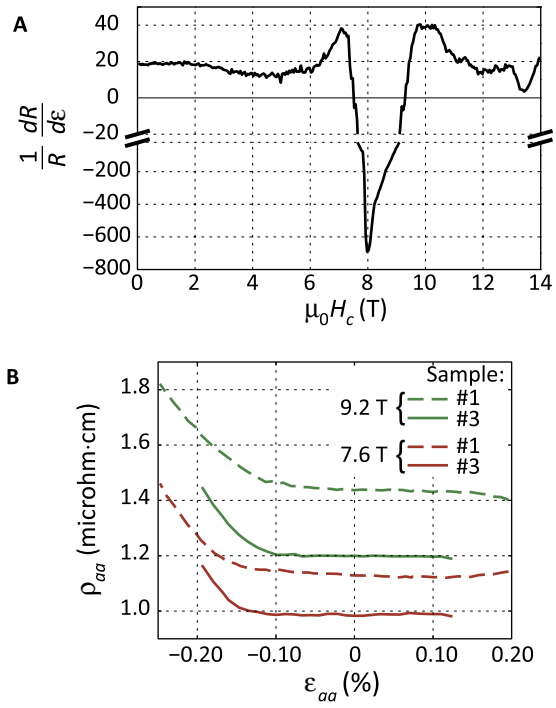

Fig. 4. Elastoresistance. (**A**) Elastoresistance $(1/R)dR/d\varepsilon$ against magnetic field for sample #1. **H** = (0, 0, H_c), $T \approx 300$ mK. (**B**) ρ_{aa} against strain at 7.6 and 9.2 T. At these fields, ρ_{aa} is nearly independent of strain over a wide range of strain.

0.9 T, allowing the field angle to be swept across a range ≈ arctan (0.9/8.5) − arctan(−0.9/8.5) = 12°. Samples were mounted on a mechanical rotator to allow the sample *c* axis to be shifted relative to this accessible range.

Three samples were measured in the vector magnet: a high–aspect ratio sample optimized for sensitivity to ρ_{aa} and two octagonal samples. The octagonal shape provides shape symmetry between the *a* and *b* axes as well as between the ⟨100⟩ and ⟨110⟩ directions, to avoid biasing possible domain structures (*45*). All samples were mounted on flexible wires to avoid strain effects. We present data from the octagons, although our conclusions are supported by all three samples independently. The contact configuration for the octagonal samples is illustrated in Fig. 5. An *a*-axis resistance is measured by applying a current through contacts 1 and 5 and measuring the voltage between contacts 2 and 4 or between contacts 8 and 6. Rotating the current and voltage contacts by 90° yields a *b*-axis resistance. With this geometry, the current flow is not perfectly homogeneous; thus, the measured *a*-axis resistance has some dependence on ρ_{bb}, and vice versa. However, whether a prominent feature is primarily due to a change in ρ_{aa} or ρ_{bb} becomes unambiguous because of the shape symmetry of the sample.

We start with a field rotation study: $R_{aa} = (V_2 - V_4)/I_{15}$ and $R_{bb} = (V_4 - V_6)/I_{37}$ were measured while rotating **H** about **c** at a fixed polar angle $\theta = 6°$. Results are shown in Fig. 5. Both quantities are found to vary smoothly and approximately as $\cos(2\phi)$. Field rotation studies on the high–aspect ratio sample for θ between 1° and 10.5° similarly showed a smooth dependence of ρ_{aa} on ϕ, approximately proportional to $\cos(2\phi)$ for θ below ~8°.

This smooth dependence of R_{aa} and R_{bb} on ϕ does not match naïve expectations for an Ising-type C_2-symmetric order parameter, for which sharp steps are expected when the orientation of the order

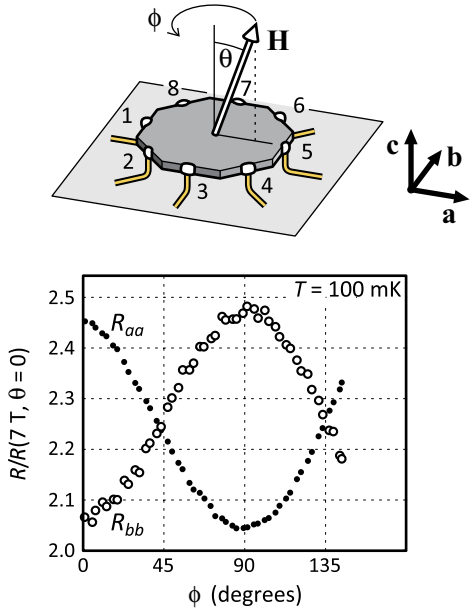

Fig. 5. Vector field sample configuration and resistance against ϕ. (**Top**) Sample and electrical contact configuration for the octagonal samples. (**Bottom**) R_{aa} and R_{bb} against ϕ, with θ fixed at 6° and $\mu_0|\mathbf{H}|$ fixed at 7.83 T. $R_{aa} = (V_2 - V_4)/I_{15}$ and $R_{bb} = (V_4 - V_6)/I_{37}$.

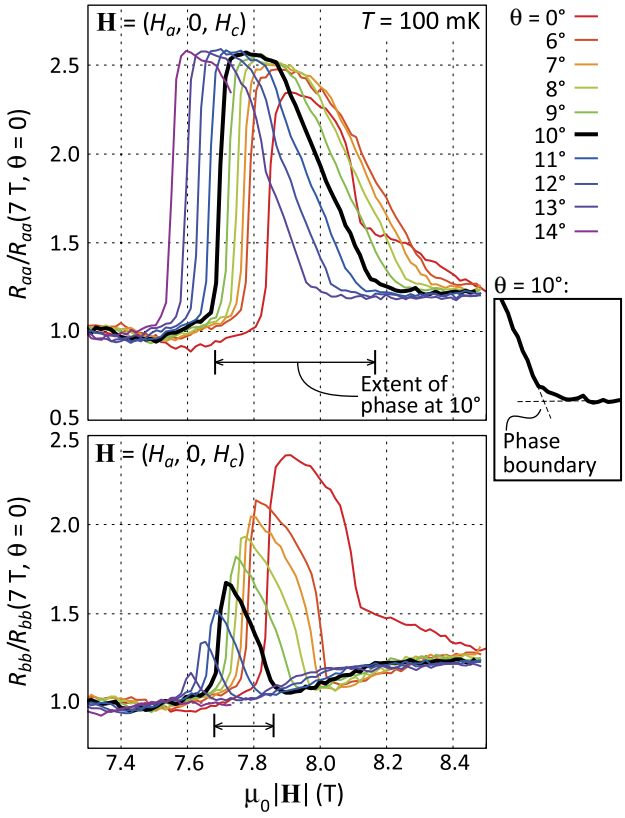

Fig. 6. Resistance against θ and |H|. R_{aa} and R_{bb} against $|\mathbf{H}|$ at various field angles $\theta = \tan^{-1}(H_a/H_c)$. $H_b = 0$, $T = 100$ mK. The phase boundaries are determined by the changes in slope, illustrated as an example for θ = 10°.

flips. However, if order of this type is broken up into domains, then the reorientation of individual domains may yield a series of smaller steps, known in ferromagnets as Barkhausen jumps, rather than a single large step. If domains are very small, then individual steps might not be visible at all, but thermal or quantum fluctuations of the domain orientation may yield observable excess noise, such as that reported in $YBa_2Cu_3O_{6+x}$ (*46*, *47*). Our measurements on $Sr_3Ru_2O_7$ resolved neither Barkhausen-like jumps nor excess noise. This is notable evidence against an Ising-type C_2-symmetric order, especially because the very low disorder of the sample means that a fine-scale domain structure is not generally expected. However, this evidence is not conclusive on its own because it might be an issue of experimental resolution.

The cos(2ϕ) form of R_{aa} and R_{bb} is consistent with a quadratic coupling to the in-plane field. In the absence of in-plane ferromagnetism, the response to the in-plane field should be symmetric with respect to the sign of the field; thus, for small in-plane fields where a lowest-order expansion applies, one generally expects $R_{aa} = R_{aa,0} + aH_a^2 + bH_b^2 = R_{aa,0} + H^2(a\cos^2\phi + b\sin^2\phi)\cos^2\theta$, where $R_{aa,0}$ is the resistance with $H_a = H_b = 0$, and a and b are coupling constants. A cos 2ϕ variation of R_{aa} results when $a \neq b$.

To complement the strain data shown in Figs. 2 and 3, we mapped R_{aa} and R_{bb} against H_a and H_c (keeping $H_b = 0$). R_{aa} was measured while sweeping $|\mathbf{H}|$ through the phase at fixed θ, and then R_{bb} was measured in a second $|\mathbf{H}|$ sweep at the same θ. θ was incremented outside the field range of phase formation, to minimize the chances of creating metastable domain structures in the case of a spontaneously C_2-symmetric order. Results of measurements at nine nonzero values of θ are shown in Fig. 6, and contour plots of R_{aa} and R_{bb} are presented in Fig. 7A. The vector field and strain measurements are complementary, because although achievable strains can much more strongly perturb the phase than the in-plane field, the transitions are sharper in the vector field data; thus, the overlap region identified in the strain data might be resolved more clearly in the vector field data. The transitions can be readily identified by changes in slope of R against $|\mathbf{H}|$, as illustrated in Fig. 6. On the contour plots shown in Fig. 7A, the transitions are indicated by black points, linked as a guide to the eye by black lines. Following the quadratic dependence on the in-plane field found in Fig. 5, the data are plotted against H_a^2. The regions of enhanced R_{aa} and R_{bb}, bounded by the transitions, are shown together in Fig. 7B. Similar to the strain phase diagram (Fig. 3C), there is a region of overlap where both R_{aa} and R_{bb} are enhanced, which extends out to $(\mu_0 H_a)^2 \approx (1.7\ \mathrm{T})^2$.

If the large susceptibility of the phase to the in-plane field is due to domain movement, then hysteresis might be expected when the applied field is varied. Its high precision and the absence of sample heating make the vector magnet an ideal tool to search for this hysteresis. Results of a test in which R_{bb} was measured while increasing and then decreasing H_a are shown in Fig. 8. H_c was simultaneously controlled to stay within the overlap region, up to $\mu_0 H_a \approx 1.5$ T: If the simultaneous enhancement of ρ_{aa} and ρ_{bb} within the overlap region is due to coexisting domains of (100)- and (010)-oriented orders, then exiting and reentering the phase with the strongest possible in-plane field should give the largest possible change in domain configuration. However, the data show no resolvable hysteresis. This test was performed at 50 mK, a factor of 20 lower than the transition temperature into the phase. Another test for hysteresis consisted of in-plane field rotations similar to those illustrated in Fig. 5, with both clockwise and counterclockwise rotations. The rotations were performed at values of θ between 6° and 14° and spanned ϕ = 45°,

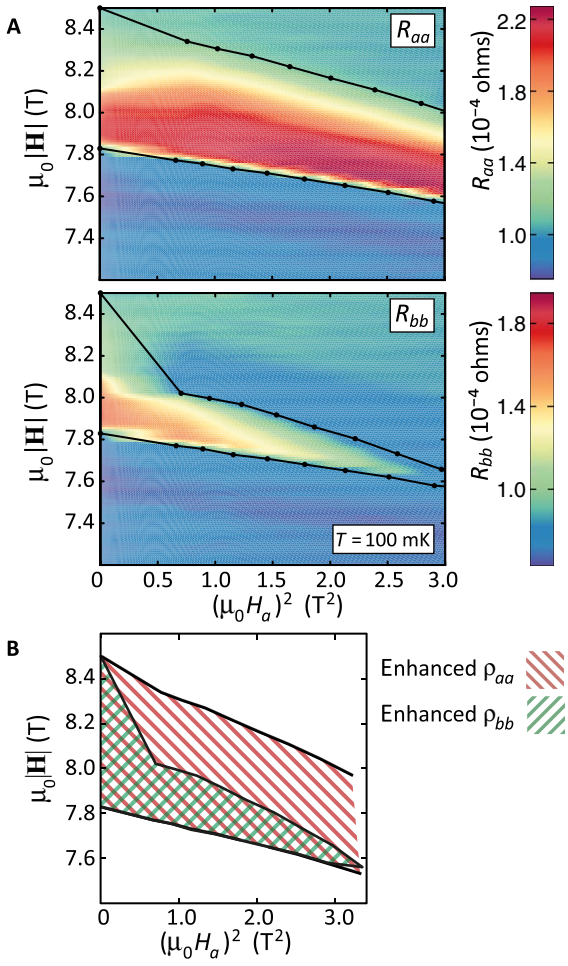

Fig. 7. Vector field results: Contour plots. (**A**) R_{aa} and R_{bb} against $|\mathbf{H}|$ and H_a^2, with $\mathbf{H} = (H_a, 0, H_c)$, at T = 100 mK. The black points are the transition points into enhanced-ρ_{aa} and enhanced-ρ_{bb} phases, determined as illustrated in Fig. 6. (**B**) Outlines of the regions of enhanced ρ_{aa} and ρ_{bb}.

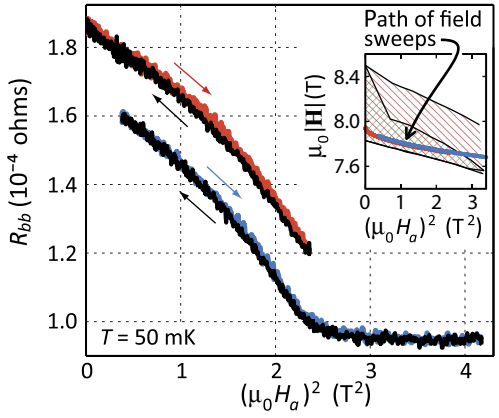

Fig. 8. Looking for hysteresis. Two demonstrations of the absence of hysteresis, in which R_{bb} was measured while increasing and then decreasing H_a. The upper curves are offset by 2×10^{-5} ohms for clarity. I = 100 μA, $\mathbf{H} = (H_a, 0, H_c)$, T = 50 mK. As shown in the inset, H_c was varied, whereas H_a was ramped to keep the sample within the enhanced ρ_{bb} phase up to $(\mu_0 H_a)^2 \approx 2.3\ T^2$.

where, in the case of spontaneous C_2 symmetry, the applied field should start to flip domains between (100) and (010) orientations. Again, no definite hysteresis was observed.

DISCUSSION

The measurements described above have confirmed the strong susceptibility of magnetotransport in $Sr_3Ru_2O_7$ to two C_2-symmetric fields: orthorhombic lattice distortion through uniaxial pressure and in-plane magnetic field. The former is a probe that has not been previously applied to $Sr_3Ru_2O_7$, whereas the vector magnetic field experiments described above have probed for hysteretic and noise signatures of domains with much higher precision than in any previous work.

Here, we first consider more carefully whether our results could be explained by domains of a C_2-symmetric order. We then briefly discuss possible forms of microscopic coexistence of density waves relevant to $Sr_3Ru_2O_7$ that could explain our data, and discuss challenges in explaining the resistivity of the anomalous phase solely with density wave order.

We believe that our results present a considerable challenge, going beyond the observed lack of hysteresis, to models that appeal to the formation and movement of domains to explain the transport properties of $Sr_3Ru_2O_7$. The basic issue is the following. In the experiments, we repeatedly entered and exited the phase in the presence of nonzero C_2 field, so that any domain configuration should be at or near the ground state under the applied C_2 field. For domains to account for the resistive properties of $Sr_3Ru_2O_7$, they must persist to at least the upper limits of the overlap regions. As shown in Figs. 3C and 7B, this means that domains should exist, in the ground state, in strains up to $\sim 4 \times 10^{-4}$ and in-plane fields up to ~1.7 T. For this to be the case, there must be a free energy minimum for domain formation that is stronger than an interaction energy related to symmetry-breaking fields of these strengths. Examination of simple candidate mechanisms illustrates the difficulty with this approach.

One possible mechanism for ground-state domain formation is long-range interactions, which may be elastic or magnetic. If C_2-symmetric electronic order induces C_2 lattice deformation that exceeds the applied average strain, then domain formation would reduce the total elastic energy of the system. The domain walls would be closely analogous to twin boundaries of an orthorhombic lattice (*24*). However, this mechanism is not quantitatively consistent with observations. The lattice distortion resulting from in-plane fields high enough to saturate the resistive anisotropy is known to be $\sim 4 \times 10^{-6}$ (*48*). That is, if the phase is spontaneously C_2-symmetric, then elastic interactions would favor domain formation only up to an applied average strain of $\sim 4 \times 10^{-6}$, which is two orders of magnitude less than the observed extent of the overlap region (up to strains of $\sim 4 \times 10^{-4}$). Similarly, long-range magnetic interactions could favor domain formation if the domains have differing magnetizations (*49*). However, the order would need to include in-plane ferromagnetism on at least a scale of ~1.7 T to stabilize domains against an applied in-plane field of 1.7 T, and there is no expectation of that. For comparison, the larger metamagnetic jump (at 7.9 T) has a magnitude of $\mu_0 \Delta M = 0.008$ T (*35*).

Another possible mechanism is random-field disorder, which could result, for example, from locally oriented defects or inhomogeneous strain. A C_2-symmetric order might have domains in the ground state if an internal disorder field has spatially varying orientation. In this case, as the in-plane field is ramped, the ground-state domain distribution should generally transition smoothly from all-(100) to

all-(010), with the width of the transition determined by the distribution of internal fields. Hysteresis and glassy dynamics are also possible, especially if the disorder has a short length scale (*47*). However, in both the strain and vector field data the transitions into the overlap regions are sharp in comparison with the width of the overlap, which is against expectations for strong disorder broadening. This is shown particularly in Fig. 8, where the form of $R_{aa}(H_a)$ is much more consistent with a transition at $(\mu_0 H_a)^2 \approx 2.4\ \mathrm{T}^2$ than with disorder broadening of a (100)-to-(010) transition at $H_a = 0$.

The above analysis is based on specific mechanisms for domain formation, but the central issue is more general: Any domains present in the system have not only to be stable against substantial C_2 fields but also to be associated with extremely weak hysteresis, below the resolution of our measurements. In general, these are contradictory requirements.

Given the rather strong arguments against the presence of domains in the anomalous state, the most natural conclusion is that the observed resistivity in the phase is the intrinsic resistivity, not a result of domain wall scattering. Further, our data and analysis argue for the intrinsic order being multicomponent, with microscopic coexistence of (100)- and (010)-oriented components when applied C_2 fields are not too large. The argument that high resistivity is an intrinsic property of the phase is supported by the fact that strong resistive anisotropy and strong resistivity enhancement along the "hard" direction persist even under strong C_2 fields, where samples have been argued to be monodomain (*34*, *48*).

With the above conclusions in mind, the close correlation observed in the neutron scattering data of Lester *et al.* (*34*) between spin density wave order and resistivity in the anomalous phase means that the simplest hypothesis is to associate the two components with spin density waves. We cannot rule out the possibility that the spin modulations observed in the neutron experiments are connected with further, as-yet unobserved, charge order, but any discussion of this would be speculative in the absence of concrete observations in the charge sector.

In the scenario where resistivity is directly linked to spin density wave formation, there are several possibilities for microscopic coexistence. The simplest is that the (100)- and (010)-oriented waves coexist within each layer, yielding a checkerboard-type order, perhaps similar to the tetragonal spin density wave state recently discovered in iron pnictide superconductors (*50*). The coexistence could also be microscopic but spatially separated, with the (100) and (010) components existing in alternate layers within each bilayer, yielding an inversion-symmetry–broken state. This would be similar to the intralayer nematic order discussed by Puetter *et al.* (*51*), Yamase (*52*), and Hitomi and Yanase (*53*), where it is proposed that $Sr_3Ru_2O_7$ could host nematic order but with the orientation of the nematicity alternating from layer to layer. Another possibility is that the (100) and (010) components exist in alternating bilayers.

Although we believe that the evidence for microscopic coexistence is strong, the high susceptibility of the phase to C_4 symmetry–breaking fields is surprising. It may reflect fine-tuning, in that the order is only weakly stable in the unstrained lattice and hence has a high general susceptibility to perturbation. However, our observations could also reflect a more specific high susceptibility toward C_2 symmetry, for example, if the (100) and (010) components compete reasonably strongly but not strongly enough to prevent microscopic coexistence. Another possibility is that, if the (100) and (010) components alternate between layers or bilayers, then the coupling that stabilizes this alternation is likely to be weak, such that the density waves might reorient with modest applied C_2 fields. In general, it would be interesting to determine whether there is a deeper reason for the high perturbability of the phase. We also note that the strong enhancement of the phase with strain could have bearing on studies of the links between phase formation and metamagnetic quantum criticality: Under strains above ~0.1%, the region of phase formation appears to extend to fields considerably above the metamagnetic transitions. We believe that this is a point that deserves further study.

Finally, we note that although our data are qualitatively inconsistent with a domain scenario, an outstanding challenge to any model not relying on strong domain wall scattering is to understand the magnitude of the resistivity enhancement. We have proposed direct identification of ρ_{aa} and ρ_{bb} enhancements with magnitudes of (100)- and (010)-oriented order parameter components, that is, the intrinsic resistivity of the ordered phase without observable domain wall scattering. This model provides a qualitatively simple explanation for our data. However, the scale of the resistive change is not easy to understand. At large strains, the ratio of resistivities parallel and perpendicular to the density wave $\rho_{\parallel}/\rho_{\perp}$ is ~2.4. For comparison, in elemental chromium, a 3D metallic spin density wave system with $T_N = 312$ K, $\rho_{\parallel}/\rho_{\perp}$, saturates at only 1.08 (*54*). $Sr_3Ru_2O_7$ has at least seven Fermi surface sheets (*17*), and it does not appear possible that nesting across a single wave vector could gap away enough carriers to yield this strong anisotropy. Widespread gapping also appears inconsistent with observed thermodynamic properties: The entropy and specific heat are highest in the region of phase formation (*35*, *55*, *56*), indicating a large number of ungapped carriers. If the observed resistivity is intrinsic and not due to domain wall scattering (as the experiments reported here suggest), then understanding the magnitude of the changes in resistivity is a key issue for future investigations of $Sr_3Ru_2O_7$.

MATERIALS AND METHODS

Samples were grown by means of a floating zone method (*57*) and cut to the desired shape with a wire saw. The strained samples were 40 to 45 μm thick and 170 to 280 μm wide. Electrical contacts were made with DuPont 6838 silver paste and cured at 450°C for ≈5 min. The strained samples were secured in the strain apparatus with Stycast 2850, which was cured at a temperature of ≈65°C for several hours to obtain a harder cure than at room temperature. For strained samples #1, #2, and #3, the epoxy thickness was ≈80, 40, and 20 μm, respectively. For low-noise measurements of resistivity on strained sample #1 and for the vector field data, we used low-temperature transformers to amplify the signal voltage. For samples #2 and #3, room temperature transformers were used.

Strained sample #1 was mounted in the same strain apparatus reported by Hicks *et al.* (*41*, *58*), which used a strain gauge for measurement of the displacement applied to the sample. Samples #2 and #3 were mounted in a newer apparatus with a capacitive displacement sensor. Through comparison of the elastoresistive response outside the region of phase formation, it was found that strains reported from the original apparatus needed to be multiplied by a factor of 1.6 to match those from the newer apparatus, suggesting that the strain gauge somewhat impeded the motion of the original apparatus. This correction factor was verified with measurements on Sr_2RuO_4 and is included in strains reported here for sample #1. All strains reported in this paper were also corrected for an estimate of the epoxy deformation: Through finite element calculations, we estimated that 52, 68, and 78% of the applied displacement were transmitted as sample strain to the exposed portion of samples

#1, #2, and #3, respectively. In these calculations, we took the Young's modulus of the epoxy to be 15 GPa, and for $Sr_3Ru_2O_7$, we took the elastic tensor of Sr_2RuO_4 (*59*). Uncertainty in dimensions and elastic properties give an approximately 20% proportional error on all strains quoted in this study. No hysteresis against applied displacement was observed, indicating that the epoxy deformation was always elastic. Because of the field dependence of the temperature sensor, the temperature of the strained samples varied by ≈20 mK between 7 and 10 T.

SUPPLEMENTARY MATERIALS

Supplementary material for this article is available at http://advances.sciencemag.org/cgi/content/full/3/2/e1501804/DC1

fig. S1. Longitudinal response and transverse response for strained sample #2.

REFERENCES AND NOTES

1. Y. Ando, K. Segawa, S. Komiya, A. N. Lavrov, Electrical resistivity anisotropy from self-organized one dimensionality in high-temperature superconductors. *Phys. Rev. Lett.* **88**, 137005 (2002).
2. V. Hinkov, D. Haug, B. Fauqué, P. Bourges, Y. Sidis, A. Ivanov, C. Bernhard, C. T. Lin, B. Keimer, Electronic liquid crystal state in the high-temperature superconductor $YBa_2Cu_3O_{6.45}$. *Science* **319**, 597–600 (2008).
3. J.-H. Chu, J. G. Analytis, K. De Greeve, P. L. McMahon, Z. Islam, Y. Yamamoto, I. R. Fisher, In-plane resistivity anisotropy in an underdoped iron arsenide superconductor. *Science* **329**, 824–826 (2010).
4. J.-H. Chu, H.-H. Kuo, J. G. Analytis, I. R. Fisher, Divergent nematic susceptibility in an iron arsenide superconductor. *Science* **337**, 710–712 (2012).
5. J. Pollanen, K. B. Cooper, S. Brandsen, J. P. Eisenstein, L. N. Pfeiffer, K. W. West, Heterostructure symmetry and the orientation of the quantum Hall nematic phases. *Phys. Rev. B* **92**, 115410 (2015).
6. M. P. Lilly, K. B. Cooper, J. P. Eisenstein, L. N. Pfeiffer, K. W. West, Evidence for an anisotropic state of two-dimensional electrons in high Landau levels. *Phys. Rev. Lett.* **82**, 394–397 (1999).
7. R. Okazaki, T. Shibauchi, H. J. Shi, Y. Haga, T. D. Matsuda, E. Yamamoto, Y. Onuki, H. Ikeda, Y. Matsuda, Rotational symmetry breaking in the hidden-order phase of URu_2Si_2. *Science* **331**, 439–442 (2011).
8. S. Yonezawa, K. Tajiri, S. Nakata, Y. Nagai, Z. Wang, K. Segawa, Y. Ando, Y. Maeno, Thermodynamic evidence for nematic superconductivity in $Cu_xBi_2Se_3$. *Nat. Phys.* 10.1038/nphys3907 (2016).
9. A. P. Mackenzie, J. A. N. Bruin, R. A. Borzi, A. W. Rost, S. A. Grigera, Quantum criticality and the formation of a putative electronic liquid crystal in $Sr_3Ru_2O_7$. *Physica C* **481**, 207–214 (2012).
10. S. A. Grigera, P. Gegenwart, R. A. Borzi, F. Weickert, A. J. Schofield, R. S. Perry, T. Tayama, T. Sakakibara, Y. Maeno, A. G. Green, A. P. Mackenzie, Disorder-sensitive phase formation linked to metamagnetic quantum criticality. *Science* **306**, 1154–1157 (2004).
11. R. A. Borzi, S. A. Grigera, J. Farrell, R. S. Perry, S. J. S. Lister, S. L. Lee, D. A. Tennant, Y. Maeno, A. P. Mackenzie, Formation of a nematic fluid at high fields in $Sr_3Ru_2O_7$. *Science* **315**, 214–217 (2007).
12. M. P. Allan, A. Tamai, E. Rozbicki, M. H. Fischer, J. Voss, P. D. C. King, W. Meevasana, S. Thirupathaiah, E. Rienks, J. Fink, D. A. Tennant, R. S. Perry, J. F. Mercure, M. A. Wang, J. Lee, C. J. Fennie, E.-A. Kim, M. J. Lawler, K. M. Shen, A. P. Mackenzie, Z.-X. Shen, F. Baumberger, Formation of heavy d-electron quasiparticles in $Sr_3Ru_2O_7$. *New J. Phys.* **15**, 063029 (2013).
13. S.-I. Ikeda, Y. Maeno, S. Nakatsuji, M. Kosaka, Y. Uwatoko, Ground state in $Sr_3Ru_2O_7$: Fermi liquid close to a ferromagnetic instability. *Phys. Rev. B Condens. Matter Mater. Phys.* **62**, R6089–R6092 (2000).
14. L. Capogna, E. M. Forgan, S. M. Hayden, A. Wildes, J. A. Duffy, A. P. Mackenzie, R. S. Perry, S. Ikeda, Y. Maeno, S. P. Brown, Observation of two-dimensional spin fluctuations in the bilayer ruthenate $Sr_3Ru_2O_7$ by inelastic neutron scattering. *Phys. Rev. B Condens. Matter Mater. Phys.* **62**, 012504 (2003).
15. R. Mathieu, A. Asamitsu, Y. Kaneko, J. P. He, X. Z. Yu, R. Kumai, Y. Onose, N. Takeshita, T. Arima, H. Takagi, Y. Tokura, Impurity-induced transition to a Mott insulator in $Sr_3Ru_2O_7$. *Phys. Rev. B* **72**, 092404 (2005).
16. M. A. Hossain, B. Bohnenbuck, Y. D. Chuang, M. W. Haverkort, I. S. Elfimov, A. Tanaka, A. G. Cruz Gonzalez, Z. Hu, H.-J. Lin, C. T. Chen, R. Mathieu, Y. Tokura, Y. Yoshida, L. H. Tjeng, Z. Hussain, B. Keimer, G. A. Sawatzky, A. Damascelli, Mott versus Slater-type metal-insulator transition in Mn-substituted $Sr_3Ru_2O_7$. *Phys. Rev. B* **86**, 041102 (2012).
17. A. Tamai, M. P. Allan, J. F. Mercure, W. Meevasana, R. Dunkel, D. H. Lu, R. S. Perry, A. P. Mackenzie, D. J. Singh, Z.-X. Shen, F. Baumberger, Fermi surface and van Hove singularities in the itinerant metamagnet $Sr_3Ru_2O_7$. *Phys. Rev. Lett.* **101**, 026407 (2008).
18. S. A. Grigera, R. A. Borzi, A. P. Mackenzie, S. R. Julian, R. S. Perry, Y. Maeno, Angular dependence of the magnetic susceptibility in the itinerant metamagnet $Sr_3Ru_2O_7$. *Phys. Rev. B* **67**, 214427 (2003).
19. A. G. Green, S. A. Grigera, R. A. Borzi, A. P. Mackenzie, R. S. Perry, B. D. Simons, Phase bifurcation and quantum fluctuations in $Sr_3Ru_2O_7$. *Phys. Rev. Lett.* **95**, 086402 (2005).
20. H.-Y. Kee, Y. B. Kim, Itinerant metamagnetism induced by electronic nematic order. *Phys. Rev. B* **71**, 184402 (2005).
21. H. Yamase, Mean-field theory on a coupled system of ferromagnetism and electronic nematic order. *Phys. Rev. B* **87**, 195117 (2013).
22. A. M. Berridge, A. G. Green, S. A. Grigera, B. D. Simons, Inhomogeneous magnetic phases: A Fulde-Ferrell-Larkin-Ovchinnikov-like phase in $Sr_3Ru_2O_7$. *Phys. Rev. Lett.* **102**, 136404 (2009).
23. A. M. Berridge, S. A. Grigera, B. D. Simons, A. G. Green, Magnetic analog of the Fulde-Ferrell-Larkin-Ovchinnikov phase in $Sr_3Ru_2O_7$. *Phys. Rev. B* **81**, 054429 (2010).
24. H. Doh, Y. B. Kim, K. H. Ahn, Nematic domains and resistivity in an itinerant metamagnet coupled to a lattice. *Phys. Rev. Lett.* **98**, 126407 (2007).
25. H. Shaked, J. D. Jorgensen, O. Chmaissem, S. Ikeda, Y. Maeno, Neutron diffraction study of the structural distortions in $Sr_3Ru_2O_7$. *J. Solid State Chem.* **154**, 361–367 (2000).
26. R. Kiyanagi, K. Tsuda, N. Aso, H. Kimura, Y. Noda, Y. Yoshida, S.-I. Ikeda, Y. Uwatoko, Investigation of the structure of single crystal $Sr_3Ru_2O_7$ by neutron and convergent beam electron diffractions. *J. Phys. Soc. Jpn.* **73**, 639–642 (2004).
27. B. Hu, G. T. McCandless, M. Menard, V. B. Nascimento, J. Y. Chen, E. W. Plummer, R. Jin, Surface and bulk structural properties of single-crystalline $Sr_3Ru_2O_7$. *Phys. Rev. B* **81**, 184104 (2010).
28. J. A. N. Bruin, R. A. Borzi, S. A. Grigera, A. W. Rost, R. S. Perry, A. P. Mackenzie, Study of the electronic nematic phase of $Sr_3Ru_2O_7$ with precise control of the applied magnetic field vector. *Phys. Rev. B* **87**, 161106 (2013).
29. H. Yamase, A. A. Katanin, Van Hove singularity and spontaneous Fermi surface symmetry breaking in $Sr_3Ru_2O_7$. *J. Phys. Soc. Jpn.* **76**, 073706 (2007).
30. W.-C. Lee, C. Wu, Theory of unconventional metamagnetic electron states in orbital band systems. *Phys. Rev. B* **80**, 104438 (2009).
31. S. Raghu, A. Paramekanti, E. A. Kim, R. A. Borzi, S. A. Grigera, A. P. Mackenzie, S. A. Kivelson, Microscopic theory of the nematic phase in $Sr_3Ru_2O_7$. *Phys. Rev. B* **79**, 214402 (2009).
32. C. M. Puetter, J. G. Rau, H.-Y. Kee, Microscopic route to nematicity in $Sr_3Ru_2O_7$. *Phys. Rev. B* **81**, 081105 (2010).
33. M. Tsuchiizu, Y. Ohno, S. Onari, H. Kontani, Orbital nematic instability in the two-orbital Hubbard model: Renormalization-group + constrained RPA analysis. *Phys. Rev. Lett.* **111**, 057003 (2013).
34. C. Lester, S. Ramos, R. S. Perry, T. P. Croft, R. I. Bewley, T. Guidi, P. Manuel, D. D. Khalyavin, E. M. Forgan, S. M. Hayden, Field-tunable spin-density-wave phases in $Sr_3Ru_2O_7$. *Nat. Mater.* **14**, 373–378 (2015).
35. A. W. Rost, R. S. Perry, J.-F. Mercure, A. P. Mackenzie, S. A. Grigera, Entropy landscape of phase formation associated with quantum criticality in $Sr_3Ru_2O_7$. *Science* **325**, 1360–1363 (2009).
36. C. Stingl, R. S. Perry, Y. Maeno, P. Gegenwart, Electronic nematicity and its relation to quantum criticality in $Sr_3Ru_2O_7$ studied by thermal expansion. *Phys. Status Solidi B* **250**, 450–456 (2013).
37. W. Wu, A. McCollam, S. A. Grigera, R. S. Perry, A. P. Mackenzie, S. R. Julian, Quantum critical metamagnetism of $Sr_3Ru_2O_7$ under hydrostatic pressure. *Phys. Rev. B* **83**, 045106 (2011).
38. M. Chiao, C. Pfleiderer, S. R. Julian, G. G. Lonzarich, R. S. Perry, A. P. Mackenzie, Y. Maeno, Effect of pressure on metamagnetic $Sr_3Ru_2O_7$. *Physica B* **312–313**, 698–699 (2002).
39. S.-I. Ikeda, N. Shirakawa, T. Yanagisawa, Y. Yoshida, S. Koikegami, S. Koike, M. Kosaka, Y. Uwatoko, Uniaxial-pressure induced ferromagnetism of enhanced paramagnetic $Sr_3Ru_2O_7$. *J. Phys. Soc. Jpn.* **73**, 1322–1325 (2004).
40. H. Yamase, Electronic nematic phase transition in the presence of anisotropy. *Phys. Rev. B* **91**, 195121 (2015).
41. C. W. Hicks, M. E. Barber, S. D. Edkins, D. O. Brodsky, A. P. Mackenzie, Piezoelectric-based apparatus for strain-tuning. *Rev. Sci. Instrum.* **85**, 065003 (2014).
42. J.-F. Mercure, A. W. Rost, E. C. T. O'Farrell, S. K. Goh, R. S. Perry, M. L. Sutherland, S. A. Grigera, R. A. Borzi, P. Gegenwart, A. S. Gibbs, A. P. Mackenzie, Quantum oscillations near the metamagnetic transition in $Sr_3Ru_2O_7$. *Phys. Rev. B* **81**, 235103 (2010).
43. D. Sun, A. W. Rost, R. S. Perry, A. P. Mackenzie, M. Brando, Low temperature thermodynamic investigation of the phase diagram of $Sr_3Ru_2O_7$. Condens. Matter arXiv:1605.00396 (2016).
44. H.-H. Kuo, M. C. Shapiro, S. C. Riggs, I. R. Fisher, Measurement of the elastoresistive coefficients of the underdoped iron arsenide $Ba(Fe_{0.975}Ca_{0.025})_2As_2$. *Phys. Rev. B* **88**, 085113 (2013).

45. R. A. Borzi, A. McCollam, J. A. N. Bruin, R. S. Perry, A. P. Mackenzie, S. A. Grigera, Hall coefficient anomaly in the low-temperature high-field phase of $Sr_3Ru_2O_7$. *Phys. Rev. B* **84**, 205112 (2011).
46. D. S. Caplan, V. Orlyanchik, M. B. Weissman, D. J. Van Harlingen, E. H. Fradkin, M. J. Hinton, T. R. Lemberger, Anomalous noise in the pseudogap regime in $YBa_2Cu_3O_{7-\delta}$. *Phys. Rev. Lett.* **104**, 177001 (2010).
47. E. W. Carlson, K. A. Dahmen, E. Fradkin, S. A. Kivelson, Hysteresis and noise from electronic nematicity in high-temperature superconductors. *Phys. Rev. Lett.* **96**, 097003 (2006).
48. C. Stingl, R. S. Perry, Y. Maeno, P. Gegenwart, Symmetry-breaking lattice distortion in $Sr_3Ru_2O_7$. *Phys. Rev. Lett.* **107**, 026404 (2011).
49. B. Binz, H. B. Braun, T. M. Rice, M. Sigrist, Magnetic domain formation in itinerant metamagnets. *Phys. Rev. Lett.* **96**, 196406 (2006).
50. S. Avci, O. Chmaissem, J. M. Allred, S. Rosenkranz, I. Eremin, A. V. Chubukov, D. E. Bugaris, D. Y. Chung, M. G. Kanatzidis, J. P. Castellan, J. A. Shlueter, H. Claus, D. D. Khalyavin, P. Manuel, A. Daoud-Aladine, R. Osborn, Magnetically driven suppression of nematic order in an iron-based superconductor. *Nat. Commun.* **5**, 3845 (2014).
51. C. Puetter, H. Doh, H.-Y. Kee, Metanematic transitions in a bilayer system: Application to the bilayer ruthenate. *Phys. Rev. B* **76**, 235112 (2007).
52. H. Yamase, Spontaneous Fermi surface symmetry breaking in bilayer systems. *Phys. Rev. B* **80**, 115102 (2009).
53. T. Hitomi, Y. Yanase, Electric octupole order in bilayer ruthenate $Sr_3Ru_2O_7$. *J. Phys. Soc. Jpn.* **83**, 114704 (2014).
54. W. B. Muir, J. O. Ström-Olsen, Electrical resistance of single-crystal single-domain chromium from 77 to 325°K. *Phys. Rev. B* **4**, 988–991 (1971).
55. P. Gegenwart, F. Weickert, M. Garst, R. S. Perry, Y. Maeno, Metamagnetic quantum criticality in $Sr_3Ru_2O_7$ studied by thermal expansion. *Phys. Rev. Lett.* **96**, 136402 (2006).
56. A. W. Rost, S. A. Grigera, J. A. N. Bruin, R. S. Perry, D. Tian, S. Raghu, S. A. Kivelson, A. P. Mackenzie, Thermodynamics of phase formation in the quantum critical metal $Sr_3Ru_2O_7$. *Proc. Natl. Acad. Sci. U.S.A.* **108**, 16549 (2011).
57. R. S. Perry, Y. Maeno, Systematic approach to the growth of high-quality single crystals of $Sr_3Ru_2O_7$. *J. Cryst. Growth* **271**, 134–141 (2004).
58. C. W. Hicks, D. O. Brodsky, E. A. Yelland, A. S. Gibbs, J. A. N. Bruin, M. E. Barber, S. D. Edkins, K. Nishimura, S. Yonezawa, Y. Maeno, A. P. Mackenzie, Strong increase of T_c of Sr_2RuO_4 under both compressive and tensile strain. *Science* **344**, 283–285 (2014).
59. J. P. Paglione, C. Lupien, W. A. MacFarlane, J. M. Perz, L. Taillefer, Z. Q. Mao, Y. Maeno, Elastic tensor of Sr_2RuO_4. *Phys. Rev. B* **65**, 220506 (2002).

Acknowledgments: We acknowledge useful discussions with J. J. Betouras, E. Berg, R. M. Fernandes, A. G. Green, S. M. Hayden, C. A. Hooley, S. A. Kivelson, C. Lester, and W. Metzner. **Funding:** This work was supported by the Max Planck Society, the U.K. Engineering and Physical Sciences Research Council (grants EP/1031014/1 and EP/G03673X/1), Agencia Nacional de Promoción Científica y Tecnológica (Argentina) through Proyecto de Investigación Científica y Tecnológica 2013 N•2004 and N•2618, and Consejo Nacional de Investigaciones Científicas y Técnicas. **Author contributions:** D.O.B. and M.E.B. carried out measurements on strain tuning of $Sr_3Ru_2O_7$. J.A.N.B., R.A.B., and S.A.G. carried out the vector field measurements. R.S.P. grew the samples. A.P.M. and C.W.H. devised and supervised the project. The manuscript was drafted by C.W.H., A.P.M., D.O.B., R.A.B., S.A.G., and J.A.N.B. **Competing interests:** C.W.H. has 31% ownership of Razorbill Instruments, which has commercialized apparatus based on that used in this work. All other authors declare that they have no competing interests. **Data and materials availability:** All data needed to evaluate the conclusions in the paper are present in the paper and/or the Supplementary Materials. Data underpinning this publication can be accessed at http://edmond.mpdl.mpg.de/imeji/collection/FTJwbUj1iAnXbffX. Additional data related to this paper may be requested from the authors.

Submitted 11 December 2015
Accepted 19 December 2016
Published 3 February 2017
10.1126/sciadv.1501804

Citation: D. O. Brodsky, M. E. Barber, J. A. N. Bruin, R. A. Borzi, S. A. Grigera, R. S. Perry, A. P. Mackenzie, C. W. Hicks, Strain and vector magnetic field tuning of the anomalous phase in $Sr_3Ru_2O_7$. *Sci. Adv.* **3**, e1501804 (2017).

ScienceAdvances
AAAS

Strain and vector magnetic field tuning of the anomalous phase in $Sr_3Ru_2O_7$

Daniel O. Brodsky, Mark E. Barber, Jan A. N. Bruin, Rodolfo A. Borzi, Santiago A. Grigera, Robin S. Perry, Andrew P. Mackenzie and Clifford W. Hicks (February 3, 2017)
Sci Adv 2017, 3:.
doi: 10.1126/sciadv.1501804